Spectrochimica Acta Part A: Molecular and Biomolecular Spectroscopy 266 (2022) 120452

Contents lists available at ScienceDirect

Spectrochimica Acta Part A: Molecular and Biomolecular Spectroscopy

journal homepage: www.elsevier.com/locate/saa

Characterization of atmospheric aerosols in the Antarctic region using Raman Spectroscopy and Scanning Electron Microscopy

César Marina-Montes [a], Luis V. Pérez-Arribas [b], Jesús Anzano [a], Silvia Fdez-Ortiz de Vallejuelo [c], Julene Aramendia [c], Leticia Gómez-Nubla [c], Alberto de Diego [c], Juan Manuel Madariaga [c], Jorge O. Cáceres [b,*]

[a] Laser Lab, Chemistry & Environment Group, Department of Analytical Chemistry, Faculty of Sciences, University of Zaragoza, Pedro Cerbuna 12, 50009 Zaragoza, Spain
[b] Laser Chemistry Research Group, Department of Analytical Chemistry, Faculty of Chemistry, Complutense University of Madrid, Plaza de Ciencias 1, 28040 Madrid, Spain
[c] Department of Analytical Chemistry, Faculty of Science and Technology, University of the Basque Country UPV/EHU, Leioa, Spain

HIGHLIGHTS

- Antarctic particulate matter was captured in filters using a low volume sampler.
- An analytical methodology based on Raman spectroscopy and SEM-EDS was implemented.
- Air pollutants were found, including black carbon, polystyrene and fertilizer.
- First detection of microplastics in air from Antarctica.

GRAPHICAL ABSTRACT

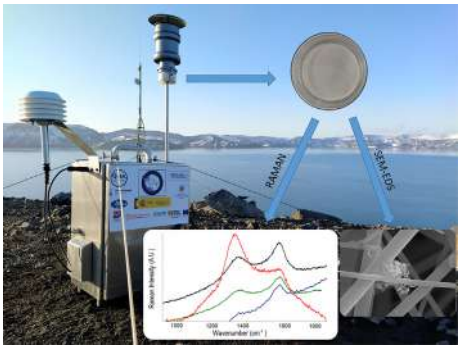

ARTICLE INFO

Article history:
Received 17 June 2021
Received in revised form 16 September 2021
Accepted 26 September 2021
Available online 29 September 2021

Keywords:
Antarctica
Atmospheric aerosols
Raman spectroscopy
Scanning electron microscopy Energy-Dispersive X-ray Spectroscopy (SEM-EDS)
Microplastics

ABSTRACT

The non-destructive spectroscopic characterization of airborne particulate matter (PM) was performed to gain better knowledge of the internal structures of atmospheric aerosols at the particle level in the Antarctic region, along with their potential sources. PM and soil samples were collected during the 2016–2017 austral summer season at the surroundings of the Spanish Antarctic Research Station "Gabriel de Castilla" (Deception Island, South Shetland Islands). PM was deposited in a low-volume sampler air filter. Raman spectroscopy (RS) and Scanning Electron Microscopy with Energy-Dispersive X-ray Spectroscopy (SEM-EDS) were used to determine the elemental and molecular composition of the individual aerosol and soil particles. Filter spectra measured by these techniques revealed long-range atmospheric transport of organic compounds (polystyrene and bacteria), local single and cluster particles made of different kinds of black carbon (BC), exotic minerals (polyhalite, arcanite, niter, ammonium nitrate, syngenite and nitrogen, phosphorus, and potassium (NPK) fertilizer), and natural PM (sea salts, silicates, iron oxides, etc.). In addition to the filter samples, forsterite and plagioclase were discovered in the soil samples together with magnetite. This is the first report of the presence of a microplastic fiber in the Antarctic air. This fact, together with the presence of other pollutants, reflects that even pristine and remote regions are influenced by anthropogenic activities.

* Corresponding author.
E-mail address: jcaceres@ucm.es (J.O. Cáceres).

https://doi.org/10.1016/j.saa.2021.120452
1386-1425/

1. Introduction

Aerosol particulate matter (PM) is a fundamental component in the atmosphere. These particles play a crucial role in the environment and health [1–3]. Firstly, aerosol particles are considered as climate drivers since they are involved in the radiative balance of the Earth, affecting the Earth́s energy budget [4]. Secondly, a strong correlation exists between hazardous heavy metals present in PM, i.e. Pb, Cd, Zn, etc., and human health-related impacts [5–6].

Atmospheric aerosols are able to travel thousands of kilometres in a limited period of time and have a typical duration of one year in the stratosphere, and one day to two weeks in the troposphere [7]. Thus, the Antarctic region, which acts as a global thermostat being one of the major pristine and isolated environments on Earth, can negatively be affected by anthropogenic PM pollution from distant as well as local sources [8]. The composition of atmospheric PM can differ widely, depending on their natural (sea, earth erosion, biogenic emissions, volcanoes, etc.) and/or anthropogenic (fossil fuel combustion, mining, agriculture, etc.) sources [9]. Among local anthropogenic sources, research stations and cruise tourism in the study area are particularly important [10]. Although aerosols have been abundantly studied in Antarctica [11–14], their variable composition is still widely unknown [7]. Thus, it is essential to investigate their chemical composition, as well as their potential sources and impacts on the Antarctic environment [15–16].

Both environmental and health effects of PM are linked to their elemental composition and their size distribution. However, these properties are not sufficient to estimate accurately their environmental consequences, since single particles are internally made up of various species. Consequently, PM chemical characterization of individual particles is needed [17–20]. Chemical characterization of individual particles through Raman spectroscopy is a powerful technique for improving the characterization of aerosols.

Raman spectroscopy (RS) is a simple rapid method which does not require sample treatment. It has been extensively used to characterize the chemical composition of airborne PM [19,21–23]. Furthermore, Raman spectra can be used to identify the potential sources of such PM, since, for instance, distinct kinds of carbonaceous particles are produced in the combustion of different fossil fuels, such as diesel, gasoline, coal or biomass burning [24–25].

In this study, RS was used to determine particle specific composition as an indicator of potential sources of Antarctic aerosol samples. As a complementary technique, and in the interest of confirming the internal structure and chemical composition of PM, analysis by scanning electron microscopy (SEM) and Energy Dispersive X-Ray Spectroscopy (EDS) were also implemented. Since RS is intended to characterize covalent compounds (carbonates, sulphates, nitrates, oxides, etc.), SEM-EDS is an appropriate complement to identify the remaining ionic particles, such as NaCl, as well as to confirm Raman analyses. The combination of these three robust techniques (RS & SEM-EDS) is perfectly adapted for identifying the chemical and structural composition of aerosol samples [26–28].

This paper focuses on the investigation by RS and SEM-EDS of the chemical composition of individual aerosol and soil particles collected during the austral summer season in the Antarctic region. This information is of great significance for studying the environmental impact of anthropogenic aerosols on the icy continent, as well as for anticipating their influence on climate change.

2. Materials and methods

2.1. Site description and sampling

Samples of atmospheric aerosols were collected from December 2016 to February 2017 on Deception Island. This island has one of Antarcticás safest harbours and is the caldera of an active volcano. It is part of the volcanic South Shetland Islands archipelago, located north of Antarctic Peninsula (Fig. 1). The Spanish Antarctic Research station "Gabriel de Castilla" (62°58′37.1″S, 60°40′32.5″W) is situated in this island together with the only other research station "Decepción" (62°58′35.7″S, 60°42′00.27″W) which belongs to Argentina. Each PM_{10} sample was collected during 24 h in circular quartz microfiber filters of 47 mm diameter (Munktell) using a low volume sampler (Derenda LVS 3.1; 2.3 m^3/h). The sampler was located (62°58′41.2″S, 60°40′39″W) about 200 and 1000 m away of the Spanish and Argentinian research stations, respectively. After the 24 h period, to avoid external contamination, the samples were meticulously stored with laboratory film in petri dishes using nitrile gloves and sterilised tweezers, and immediately transported to the research station. In total, 37 PM filter samples were collected. 5 and 3 filters were studied through RS and SEM-EDS, respectively. The European Norm was used to determine the mass concentration of each filter by gravimetry [29]. Additionally, random soil samples were collected from the soil surface (5 cm depth maximum) close to the PM sampling point, using nitrile gloves and a clean little shovel. Directly after that, soil samples were stored in polyethylene bags. In both techniques analyses (RS & SEM-EDS), no special preparation procedure was followed. These soil samples were taken in order to characterize their geochemical fingerprint to obtain spectroscopic references (mineral composition) and thus identify natural sources for the particles detected in the aerosols.

2.2. Experimental setup

RS measurements were carried out by means of a Raman InVia spectrometer (Renishaw) provided by StreamLine image tools. Spectra acquisition was done using Leica 50 × N Plan (0.75 aperture) and 20 × N Plan EPI (0.40 aperture) magnification long-range objectives. The microscope with a camera coupled used a Prior scientific motorized stage (XYZ) controlled by a joystick that facilitates focusing on and searching for points of interest. Besides,

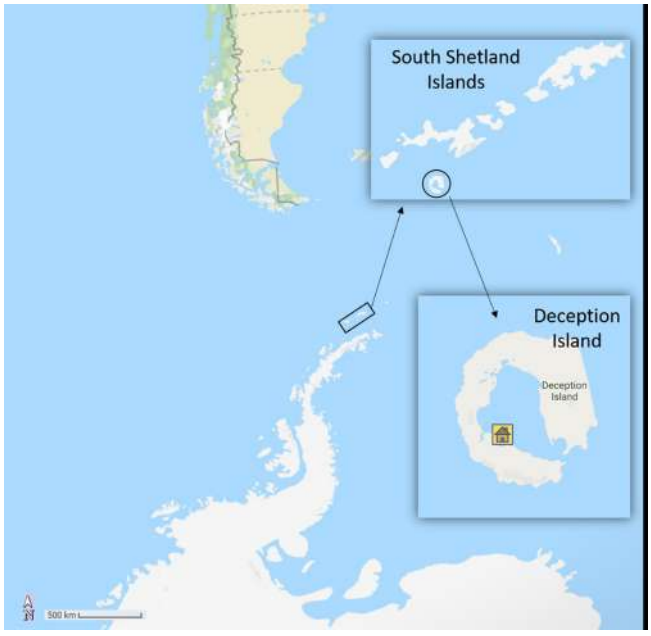

Fig. 1. Map of Deception Island with the exact location of the Gabriel de Castilla Spanish Antarctic Research Station. The yellow house shows the position of the station. Image taken from Google Earth Pro.

the device is equipped with a class 1 enclosure for avoiding artificial or sunlight effects. In addition, the instrument is installed on an antivibratory table.

In this study, RS analysis was carried out using three excitation lasers, 532 nm, 633 nm and 785 nm. The laser power was adjusted by means of density filters to below 150 μW to avoid thermodecompositions of the sample. Analyses were always performed using from 0.0001% to 10% of the power laser. Raman spectra of the cleaned filters (circular quartz microfiber filters, Munktell) were taken using all the excitation lasers in order to obtain blanks of the analytical procedure.

The calibration of the equipment was performed twice per day with a silicon slice, using its characteristic bands (520.5 cm^{-1}). The quality of measurements was assessed by an internal calibration using the same silicon chip. Moreover, the laser beam was centred twice per day to assure an appropriate analysis. The mean spectral resolution was around 1 cm^{-1}, and the spectra were obtained in a range of 100–1800 cm^{-1} or up to 3000 cm^{-1}. All the point-by-point measurements were collected using the following acquisition parameters: point analysis with a laser power of less than 10% exposure time between 2 and 10 s and between 1 and 30 accumulations. In order to improve the quality of the spectra, the measurements were set up modifying these parameters within this range.

Omnic 7.2 (Thermo Fisher-Nicolet, Madison, USA) and Wire 4.2 (Renishaw, UK) software were used for data analysis. Interpretation of the results was done by comparison of the collected Raman spectra with those of pure standard compounds from our own databases [30], the bibliography and from the RRUFF database [31].

The Raman images were collected on spots of approximately 500x500 microns. This allows performing fast 2D Raman images of the filter samples. In order to take the Raman images, the region of interest has to be defined and then an X step is performed. In this case, steps between 10 and 20 μm were used, always employing a 20x objective for the images. The methodology applied was to define as many seconds and accumulations as possible to ensure the best signal- to- noise ratio to obtain each Raman map time less than 12 h. Therefore, the acquisition conditions varied from map to map depending on the region size and the material Raman response. The most commonly applied conditions were 5–15 s and 1–5 accumulations. Once the Raman image was acquired, some automatic treatments were applied to the dataset using a systematic procedure in order to guarantee the repeatability of the experimental results. First of all, the baseline automatic correction was performed to smooth the fluorescence background in the whole spectra set. Then, cosmic ray removal was carried out using the Nearest Neighbour option which works comparing the spectrum with the nearest ones and determining correlation coefficients for each spectrum with all its spatial neighbours in order to select the most similar neighbour spectrum. In this way, as the cosmic rays are random through the comparison they would be not taken into account.

SEM filter analyses were carried out using a microscope (model HitachiS-3000 N). EDS analyses were performed with an attached EDS analyser (Oxford Instruments INCAx-sight). This SEM instrument offers the possibility to image morphological surface features of PM at high spatial resolution, down to 1 μm, with a large depth-of-field. The accelerating voltage was preset at 20 kV. The connected EDS provided elemental composition of the sample, which was limited to Z > 10.

Since this multianalytical methodology requires a reduced number of collected particles, it provides useful information about the elemental composition, size and shape of PM. Therefore, the combined technique is effective when differentiating particles originating from different sources.

2.3. Statistical analysis

PLS-Toolbox v.7.0.2 (Eigenvector Research, USA) implemented in MATLAB 2010 software (The Mathworks, MA, USA) was used on the selected Raman spectra for performing the statistical analyses such as principal component analysis (PCA).

3. Results and discussion

3.1. Raman spectra of blank filters

The composition of the clean (blanks) filters is sensitive to RS. For that reason, the Raman spectra of the filters was first measured in order to have a blank for reference. Furthermore, two blank filters were analysed by Raman. A blank spectrum is shown in Fig. 2b, where broad bands around 480, 610, 800, 980 and 1890 cm^{-1} are clearly observed due to the silicic nature of the fibers composing the filter. This spectrum was always identical in both blank filters.

3.2. Raman spectra of a microplastic in an aerosol sample

The view of the various particles through the microscope of the Raman spectrometer evidenced diverse sizes, from a couple of microns to more than 30 μm. This observation is important because in some cases the particle size was lower than the diameter of the laser spot (typically 2.5–0.8 μm when using a 50× or 20× objective, depending on the laser wavelength) used to obtain the Raman spectra. For such cases, the spectrum of the particle was obtained together with part of the background spectrum of the filter itself. This situation is shown in Fig. 2c, where the two main bands of polystyrene (at 1001 and 1602 cm^{-1}) are clearly seen together with the Raman background coming from the signals provided by the filter. In all cases, the particles of this plastic were lower in size (less than 5 μm) than the spot size of the laser and similar spectra to that shown in Fig. 2c were obtained, indicating a significant presence of microplastic particles in the filtered aerosols.

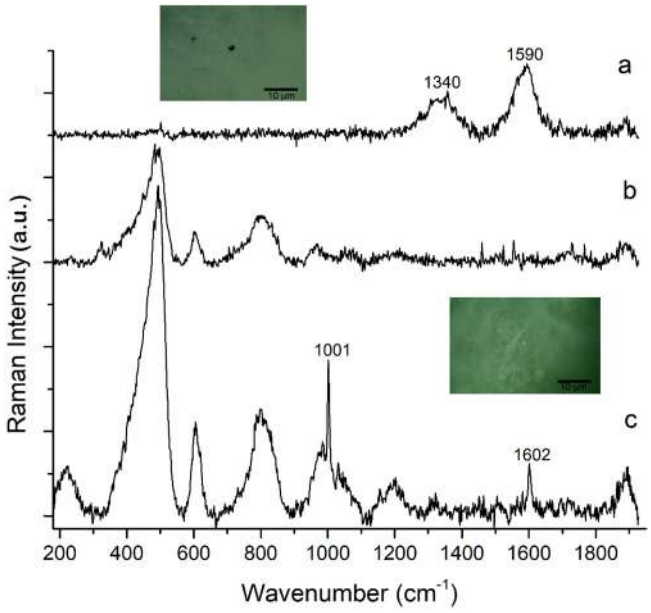

Fig. 2. Raman spectra performed on the filters a) carbon particle signal, b) filter signal and c) filter signal with a polystyrene particle signal. Spectra have been shifted for better clarity.

It is important to note that meticulous and strict measures were taken to ensure the absence of external contamination during sampling and manipulation. Additionally, strong measures and efforts are taken by Antarctic research stations to avoid possible local sources of contamination. This, together with the detection of this plastic fiber in only one of the filters (none of them blanks, neither by SEM) on a single filter region, reveals its likely anthropogenic origin from long-range atmospheric transportation. The transport of this material over long distances reaching remote regions has been previously reported [32–33], including its presence on relatively close Antarctic fresh water [34] and marine ecosystems [35–36]. Earlier investigation developed by Marina-Montes et al. [8] through the use of air-mass backward trajectories computed with the NOAA HYSPLIT 4 (HYbrid Single-Particle Lagrangian Integrated Trajectory) model, pointed out the presence of anthropogenic pollutants over Deception Island transported from the Patagonia region through the Antarctic Circumpolar wind pattern. To the best of our knowledge, for the first time, the presence of a microplastic in the Antarctic air has been reported.

3.3. Raman spectra of black carbon in aerosol samples.

Other particles were larger than the diameter of the laser spot and the focusing with the microscope could be centred on the particle without obtaining the Raman background signals from the filters. This is the case shown in Fig. 2a, where only the Raman spectrum of carbon is shown with its D and G bands. The presence of carbon particles was observed in all of the filters and in significant amounts relative to other white particles. Moreover, the Raman response of these carbon particles was different, indicating that several carbon particles (particles from different sources) were trapped by the filters. This experimental evidence led us to study in-depth the nature of such particles.

Aerosol black carbon (BC) is usually associated to anthropogenic activities such as fossil fuel and biomass combustion. The BC consists of elemental carbon and some hydrogen and oxygen. It includes different components such as soot particles, graphitic carbon and/or organic carbon coming from partially combusted biomass. Nowadays, it is considered the second most important pollutant affecting climate change.

Different aerosol BC particles were analysed and the 1050–1850 cm^{-1} range of wavenumbers of their Raman spectra were mathematically treated, using a Raman two-band fitting procedure, to determinate the different types of BC present on the filters. Fig. 3A shows four of these different Raman profiles obtained from several analysed particles. As previously described in other publications [24–25,37], there are two broad overlapping bands at ~1585 cm^{-1} and ~1360 cm^{-1}. The first band corresponds to the so-called G band, while the second band corresponds to the so-called D band or defect peak. Both bands have different forms and maximum values in their wavenumbers depending on the nature of carbon.

The Raman spectra in the above-mentioned range of four selected BC particles (named A, D, F and J in Fig. 3A) taken from the filter samples are those that exhibit greatly varying relative intensities and widths. The ratio of the D to G peaks gives the relative amount of edge to volume of the crystals [24]. The G peak is the E_{2g} mode of bulk crystalline graphite. In contrast, the D peak appears when the graphite breaks down near the crystal edges. Both peaks indicate that BC particles are formed by amorphous carbon, which is a combination of crystalline graphite and a non-graphite element. The shapes and intensities of both bands are also functions of the morphology and sample composition. The spectra of F, D and J present different shape, and the high signal intensities between the two main peaks of the observed spectra have been assigned to the G band. This band is associated with the ordered

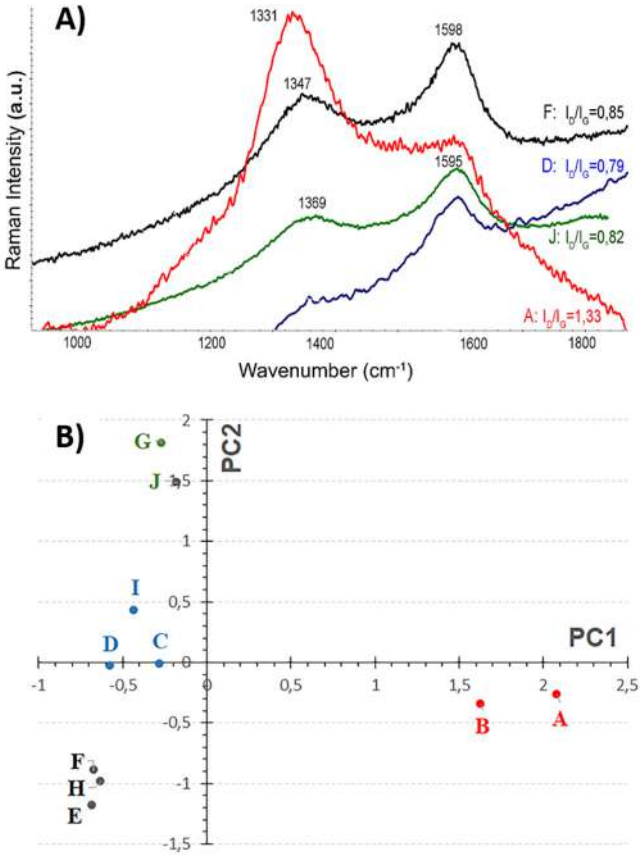

Fig. 3. A) Two-peak fitting results from Raman spectra of four BC particles (code spectra: A, D, F and J) from different Antarctic aerosol samples. B) Scores from statistical analysis from Raman spectra (Code spectra: A, B, C, D, E, F, G, H, I and J) of BC particles from PCA of two PCs.

graphitic carbon content of various compounds, such as soot, and organic molecules such as humic acids, graphite, etc.

I_D/I_G was estimated as an indicator of the degree of BC disorder [25,38]. The intensity ratios of the D band to the G band for the A spectrum (main Raman band at 1331 cm^{-1}) was higher (1.33) than the D, F and J spectra (0.79–0.85 and main Raman band at 1598 cm^{-1}). A previous study found similar values for the spectra parameter I_D/I_G, as in our D, F and J spectra, for the Raman features of carbon particles coming from biomass burning and diesel emissions [25]. In contrast, other researchers found higher I_D/I_G values for soot samples (higher or similar to those determined for sample A in this work) [38–39].

These I_D/I_G values enabled us to create Raman images from selected areas in the filters with significant abundances of BC particles. As an example, Fig. 4 shows such a Raman spectroscopy image, where the different colours (plotted as a function of the I_D/I_G values, red being the highest I_D/I_G ratios and blue the lowest) clearly show the rounded shape of the particles and how there is no zonification among them. In contrast, the different BC particles seem to be randomly trapped in the filters. However, it is still difficult to identify the different sources of the BC in this case.

Taking into account the D and G bands of the A, D, F and J spectra (see Fig. 3A), it is clear that there are different disorder levels in the analyzed BC. This indicates the existence of different kinds and sources of BC particles in the Antarctic PM sample.

In order to obtain more information about these different types of BC present in the filter samples, a chemometric analysis of the data was performed by Principal Component Analysis (PCA). PCA, as a non-supervised technique, is the most commonly used tech-

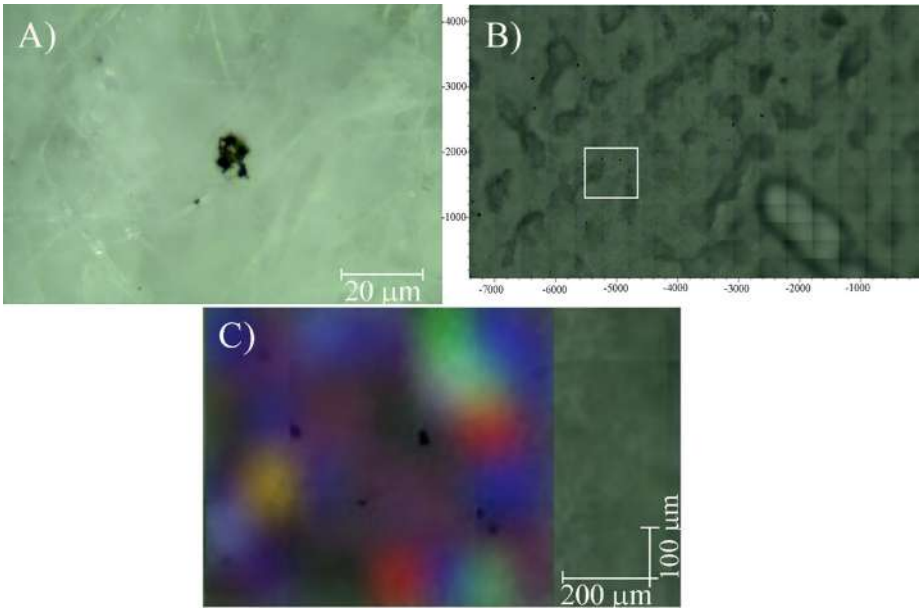

Fig. 4. A) Optical microscopic observation of a BC particle on one of the filters; B) microscopic image (×20) of the area analysed, and C) Raman imaging analysis (laser at 532 nm) of a filter showing the distribution of BC in an area of 800 × 500 microns.

nique to reduce the dimension of large datasets. Mathematically, PCA uses a covariance matrix, constructed according to the dispersion of the measured variables, to calculate the so-called "eigenvalues" and "eigenvectors". Mutually orthogonal Principal Components (PCs) are calculated by the linear combination of the original variables.

Ten spectra with only the characteristic carbon Raman bands and without the Raman background of the filter or fluorescence were selected. The selected Raman spectra were not pre-processed. The PCA was carried out using the spectral region corresponding to 1197–1663 cm^{-1}.

As the results did not significantly change when a fourth PC (only an extra 2.5% of explained variance) was considered, the model with the three first PCs (49%, 29%, and 16% of explained variance, respectively) was finally selected to describe the whole set of the Raman spectral variability in the carbon region. The scatter plot obtained is shown in Fig. 3B. This shows the representation of the scores in the space formed by two of the most important PCs. In this PCA plot, the distribution of the scores reveals the existence of at least four different behaviours of Raman spectra, which implies four different BC particles. The first one includes the A and B spectra (red ones; PC1positive value and PC2 nearly neutral), a second one for E, F and H (black ones; negative PC1 and PC2 values), a third one for C, D and I (blue ones; negative PC1 and nearly neutral PC2) and a fourth one for G and J (green ones; negative PC1 and positive PC2 values). PC1 seems to be related to the Raman intensity of the D band of BC, and PC2 to the shape and intensity of the G peaks.

Although long-range transport of BC in Antarctica cannot be discarded as previous investigations have reported [40–42], local sources likely explain the great amount of these particles found in all of the samples [43–45]. It is known that the Antarctic Peninsula and surrounding islands have a high concentration of research stations. This fact, together with the popularity of the study area as attractive Antarctic cruise destination, makes the island very influenced by local anthropogenic sources of pollution. For instance, Whalers Bay, located in the caldera of Deception Island, was the second most-visited place in the Antarctic Peninsula with more than 20,000 visitors during the 2016–2017 austral summer season [46]. However, as pointed out by Cáceres et al. [15] on his study over the same area, some other potential natural local sources of BC exist on Deception Island, such as the chinstrap penguin colonies.

Thus, taking into account that there are four different BC particles and four different potential local sources (tourist cruises, diesel generators and organic waste incineration from research stations, and penguin colonies), those particles with negative PC1 values should correspond to hydrocarbon emissions (tourist cruises, diesel generators) and penguin colonies, while the remaining BC particles correspond to organic waste incineration, characterised by Raman spectra like that named A and B.

3.4. Raman spectra of non-black carbon aerosol samples

3.4.1. Fe oxides

The search for non-BC particles in the filters revealed a great variety of sizes and shapes, alone or close to BC particles. Fig. S1 (Supplementary Materials) shows a Raman spectrum where three minerals are simultaneously present, hematite (Fe_2O_3), magnetite (Fe_3O_4) and carbon in a particle of a diameter greater than 30 μm that inhibits the appearance of the Raman background of the filter materials. The major source of Fe oxide particles in the study site is volcanic soil. Fe oxides can correspond to primary magnetite from the magmatic rocks of Deception island (magnetite) or secondary goethite in the soils created during the aerobic weathering of these rocks (hematite).

3.4.2. Syngenite, gypsum, basanite and magnesiocopiapite

Another white particle with a not rounded form, but mostly as a cluster of several grains, shown a very complex Raman spectrum as shown in Fig. S2. To decipher the minerals, present in the spectrum, the main signals around 1000 cm^{-1} were decomposed in individual bands. This mathematical treatment lead to the conclusion that syngenite ($K_2Ca(SO_4)_2{\cdot}H_2O$, Raman bands at 601, 633, 661, 982 and 1004 cm^{-1}) was present [47], together with gypsum ($CaSO_4{\cdot}2H_2O$, main Raman band at 1008 cm^{-1}) probably mixed with basanite ($CaSO_4{\cdot}½H_2O$, main Raman band at 1017 cm^{-1}) [48]. Moreover, the band at 1050 cm^{-1} shows a FWHM = 25 cm^{-1}, that belongs to nitrocalcite ($Ca(NO_3)_2{\cdot}4H_2O$) [49]. The origin of

these minerals can be attributed to the hydrothermal and volcanic activity of the island.

Another commonly detected Raman spectrum is that shown in Fig. S3. Again, to solve the complex features, the broad bands were mathematically treated to decompose in individual bands. The main Raman signal is made up of three bands that correspond to magnesio-cocapite ($MgFe_4^{3+}(SO_4)_6(OH)_2{\cdot}20H_2O$, main Raman bands at 1002 and 1025 cm^{-1}) and gypsum + bassanite due to the signal at 1011 cm^{-1}. The most important secondary broad band was also decomposed, observing several bands that indicate the presence of magnesiocopiapite and a mixture of gypsum and basanite [48,50].

3.4.3. Complex mineral

A complex Raman spectrum obtained on a white particle is shown in Fig. 5. To decipher the minerals, present in the spectrum, the main signals were decomposed in individual bands. It contains a mixture of Fe-polyhalite ($K_2FeCa_2(SO_4)_4{\cdot}2H_2O$; Raman bands at 437, 474, 635, 659, 982 and 1010 cm^{-1}), the potassium sulphate arcanite (K_2SO_4; Raman bands at 454, 612, 983 cm^{-1}) and niter (KNO_3) with a Raman band at 1049 cm^{-1} with a FWHM = 10 cm^{-1} [51]. The bands at 233, 318, 349, 558 and 788 are close to secondary bands of complex phosphate compounds, its main Raman band overlapped by the feature at 982 cm^{-1}. The sulphate bands were the most intense, followed by the nitrate band.

Apart from the above-mentioned compounds, the complicated mixture of bands suggests that the presence of methanesulfonate (MSA) also has to be considered. Na methanesulfonate shows Raman bands at 354, 560, 781, 986, 1052, among others [52].

The repeated identification of the three bands at 983, 1004–1010 and 1050 always together in the particles led to the conclusion that they have the same origin. Fertilizers display these three bands, attributed to potassium nitrate, urea, and potassium sulphate. The relative intensity of the three bands is different for each fertilizer, depending on the manufacture process and of the labelled NPK composition (% of nitrogen, phosphorous, sulphur, and potassium) [53]. However, several studies of Antarctic and Arctic particles using Raman spectroscopy have shown similar spectra with bands at ~985, 1008–1010 and 1050 cm^{-1} [22,54]. Unfortunately, there is no agreement about the actual composition or the source of the detected compounds. Some references relate the presence of sulphates and nitrates to high phytoplankton activity, mainly in summer [22,55]. Others [54], in contrast, point to the reaction between sea spray aerosol and acid gases (HNO_3 and HSO_4) as the trigger for the formation of these salts. Additionally, these compounds may have their natural origin in the volcanism of the island. Besides, the erosion of sulphate- rich soils should also be considered [56].

3.4.4. Bacteria

Fig. 6 shows a singular Raman spectrum with intense generic bands with contributions from proteins (amino acids) and lipids, such as 622 (Phenylalanine), 643 (Tyrosine), 759 (tryptophan), 830 (Tyrosine), 853 (Tyrosine), 1003 (Phenylalanine), 1127 (C-N, C-C stretching in proteins), 1200–1300 cm^{-1} (Amida III), 1447 (CH_2 deformation for lipids) and 1669 (Amide I) cm^{-1}. These were identified in the Raman spectra suggesting the presence of a possible bacteria, as described in the literature [57–58]. Raman spectra of bacterial species can be arduous to distinguish. Comparison of the spectrum of Fig. 6 with the bacteria spectra obtained by Ho et al. showed a correlation [58]. However, it did not allow the bacterial identification of the Antarctic filter sample. Since the bacteria was just identified in one filter and the complete characterization of this bacteria requires sequencing, its potential source cannot be estimated. These airborne microorganisms may be transported thousands of kilometres by atmospheric winds [59–61], being marine and terrestrial environments the most common sources. Thus, the long-range atmospheric transportation of bacteria seems to be an explanation of its presence.

3.5. Raman spectra of soil samples

Raman analyses were also performed on the Antarctic soil samples, aiming to detect some of the minerals found in the particles trapped in the filters. By this means, mainly silicates were found.

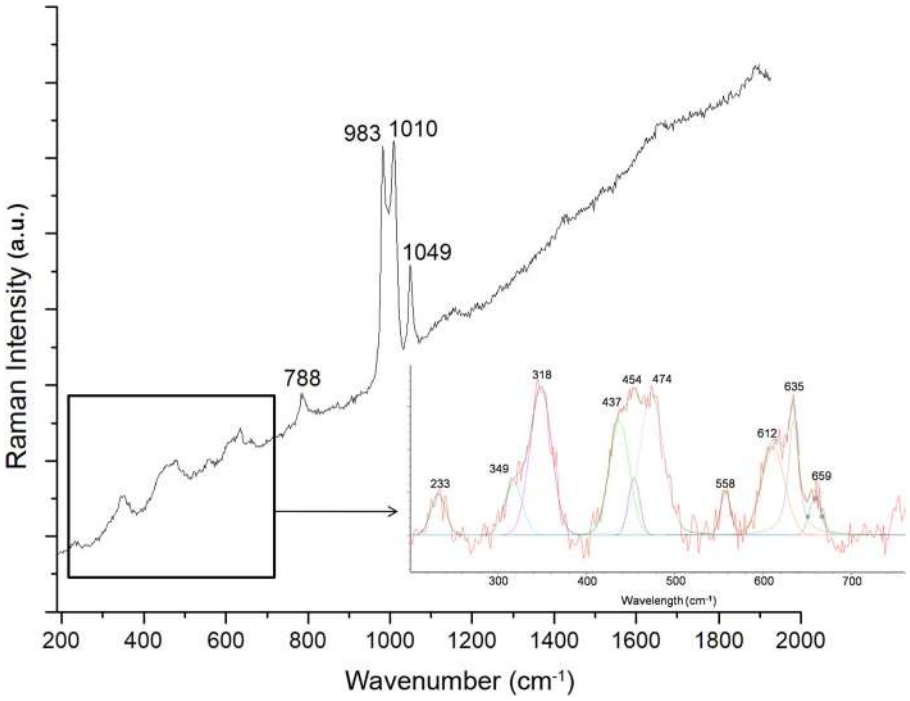

Fig. 5. Raman spectrum of a white particle containing Iron-Polyhalite, arcanite and niter from an Antarctic aerosol sample.

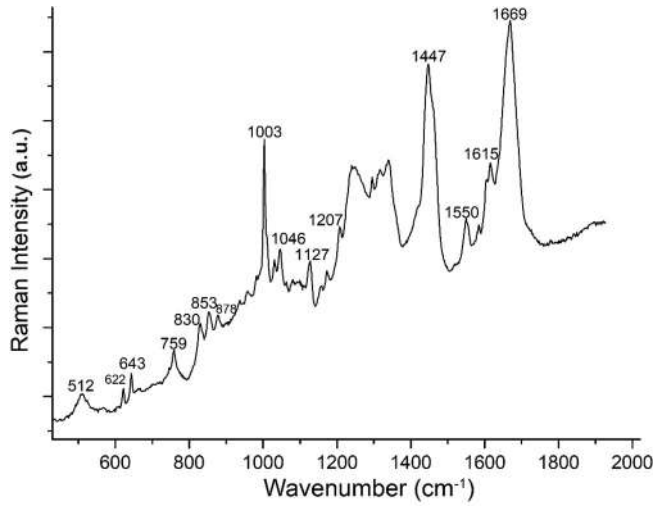

Fig. 6. Raman spectrum of a possible biological (bacteria) particle from Antarctic filter sample.

For instance, the olivine mineral forsterite (Mg_2SiO_4) was identified through its main Raman peaks at ~820 and ~854 cm^{-1} (Fig. 7). Additionally, plagioclase ($(Na,Ca)(Si,Al)_4O_8$) was also detected due to its main Raman bands at 475, 510 and 999 cm^{-1}. Finally, the iron oxide magnetite (Fe_3O_4) was detected in the soil by means of its main Raman band at 669 cm^{-1}. From these mineral phases, only magnetite was detected in the filters, but the silicate minerals cannot be discarded because the siliceous nature of the filters can inhibit critical Raman signals of silicates that could eventually be trapped.

3.6. SEM-EDS analyses of filter samples

The results obtained by SEM-EDS analyses show the presence of particles with different elemental compositions. A general morphological overview of the shapes of the particles found in the filters is presented in Fig. S4A in the Supplementary Materials. Different particles with variable compositions were detected. The EDS analyses of these strains provided the elemental composition in percentage weight of each element for four of these particles (Table S1).

According to the % values presented in Table S1, a tentative mineral composition was proposed and compared with the Raman observations previously described. On the basis of the chemical composition and shape of PM obtained through these analyses, the particles were divided into two groups: anthropogenic and natural.

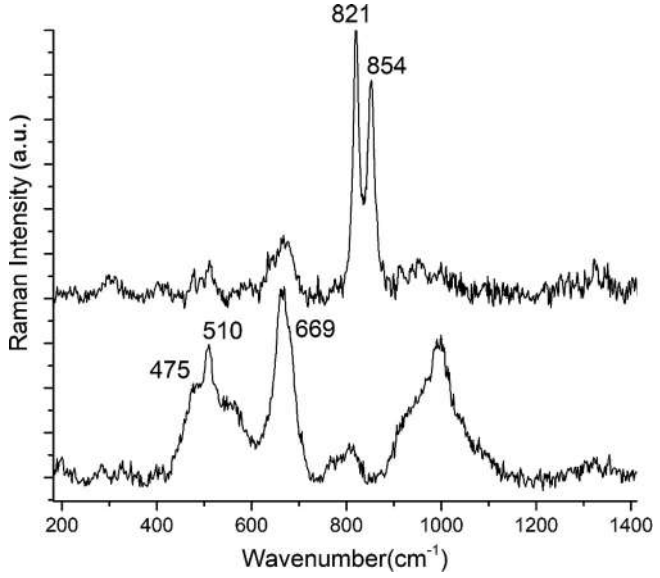

Fig. 7. Raman spectra of an olivine mineral with the typical double bands at 821 and 854 cm^{-1}, and of a plagioclase together with magnetite (band at 669 cm^{-1}).

3.6.1. Anthropogenic.

As previously stated BC particles have their origin in local emissions, particularly in the incomplete combustion of diesel and biomass burning. The shape of these particles depends on different aspects, such as the burning conditions and fuel type. As observed by SEM (Fig. S4B, these soots are made up of multiple small spheres of carbon. The major contribution was from elements such as C, Si and O, whereas Na, Cl and Mg were also present in very small concentrations (Table S1B). The contribution of Si and O corresponds to the quartz fiber filters; therefore, the most significant element is C.

3.6.2. Natural.

In the study, natural sources of PM include sea salt and crustal dust. These particles were mostly composed of sodium chloride, quartz and iron oxides.

3.6.2.1. Sodium Chloride. The elements detected, such as Na and Cl, are related to the presence of sea salts. Sodium chloride particles and their characteristic tablet-like shape, are shown in Fig. S4C Supplementary materials. They account for most of the particles collected on the filters. These particles were not detected by RS because this technique is not sensitive to ionic bonds.

3.6.2.2. Quartz (Silicate minerals). Si and O were detected in the clusters. As shown in Table S1D, the proportion of Si and O does not correspond to the SiO_2 from the quartz fiber filters; this suggests the presence of silicates (Fig. S4D in the air of the island. These particles have their origin in the resuspension of the volcanic basalt soil on the island. As shown in Table S1D, they are basically Si and O, with traces of Na and Cl. As stated before, these particles are hard to detect clearly due to the interference of the filters, but their presence has been confirmed.

3.6.2.3. Fe Oxides. Fig. S4E shows a Fe Oxide particle. These particles were rich in Fe and O with traces of elements such as Na, Mg, Si, Cl, Cu, and Ca (Table S1E). Additionally, important amounts of C, Al and Ti were found. As previously mentioned, the origin of the particles is the volcanic soil on Deception Island. RS has detected both iron oxides, hematite and magnetite, in agreement with the SEM-EDS results.

4. Conclusions

Raman analysis demonstrated the presence of microplastic fibers (polysterene), along with other anthropogenic (black carbon), biological (bacteria) and mineral (polyhalite, arcanite, niter, ammonium nitrate, syngenite and NPK fertilizer) aerosols in filter samples from Deception Island. To the best of our knowledge, these are the first aerosol measurements of microplastic particles in the Antarctic atmosphere. Furthermore, the potential source of these aerosols was studied, revealing four different local anthropogenic sources for black carbon particles, together to a likely long-range atmosphere transportation for microplastic and bacteria particles. Besides, Scanning Electron Microscopy and Energy Dispersive X-

ray spectrometry analysis of filter samples confirmed the existence and the composition of these local black carbon aerosols, as well as the presence of some others with a natural origin (sea salts, silicates and iron oxides). Finally, Raman analysis of soil samples was also implemented to confirm the local source of mineral aerosols (iron oxides, etc.).

Air pollution caused by the presence of anthropogenic particles (microplastics, BC and fertilizers) can cause serious environmental problems for the Antarctic ecosystems and climate. For instance, the presence of fertilizer particles together with the increasing trend of higher temperatures in the Antarctic Region will allow alien species to more successfully invade the Antarctic ecosystems. This disturbance, in addition to affecting the native Antarctic flora, will undoubtedly also affect the fauna. This investigation demonstrates that environmental pollution is a fact in the Antarctic region. Thus, successful characterization and regular monitoring of single particles is crucial for a better understanding of their potential environmental impacts on the Antarctic region.

CRediT authorship contribution statement

César Marina-Montes: Conceptualization, Methodology, Formal analysis, Writing – original draft, Writing – review & editing. **Luis V. Pérez-Arribas:** Conceptualization, Methodology, Formal analysis, Writing – original draft, Writing – review & editing. **Jesús Anzano:** Conceptualization, Methodology, Formal analysis, Writing – original draft, Writing – review & editing, Project administration, Funding acquisition, Supervision. **Silvia Fdez-Ortiz de Vallejuelo:** Methodology, Formal analysis, Writing – original draft. **Julene Aramendia:** Methodology, Formal analysis, Writing – original draft. **Leticia Gómez-Nubla:** Methodology, Formal analysis, Writing – original draft. **Alberto de Diego:** Methodology, Formal analysis, Writing – original draft. **Juan Manuel Madariaga:** Methodology, Formal analysis, Writing – original draft. **Jorge O. Cáceres:** Conceptualization, Methodology, Formal analysis, Writing – original draft, Writing – review & editing, Project administration, Funding acquisition, Supervision.

Declaration of Competing Interest

The authors declare that they have no known competing financial interests or personal relationships that could have appeared to influence the work reported in this paper.

Acknowledgements

The authors gratefully acknowledge the following Spanish universities for facilities and material resources: University of Zaragoza, Complutense University of Madrid and University of the Basque Country. This project forms part of the Spanish Ministry of Science research program (CTM2017-82929-R) in collaboration with the Government of Aragon proposal E23_17D and E49_20R. CMM's work was funded through a predoctoral contract (FPI) granted by the Spanish Government. Financial support from the European Social Fund & University of Zaragoza is acknowledged. The authors thank the military staff at the Gabriel de Castilla Spanish Antarctic research station for help with the installation of equipment and sample collection. Fig. 1 has been taken from Google Earth Pro.

Appendix A. Supplementary material

Supplementary data to this article can be found online at https://doi.org/10.1016/j.saa.2021.120452.

References

[1] J.T. Bates, T. Fang, V. Verma, L. Zeng, R.J. Weber, P.E. Tolbert, J.Y. Abrams, S.E. Sarnat, M. Klein, J.A. Mulholland, A.G. Russell, Review of acellular assays of ambient particulate matter oxidative potential: methods and relationships with composition, sources, and health effects, Environ. Sci. Technol. 53 (2019) 4003–4019.
[2] S. Fuzzi, U. Baltensperger, K. Carslaw, S. Decesari, H. Denier van der Gon, M.C. Facchini, D. Fowler, I. Koren, B. Langford, U. Lohmann, E. Nemitz, S. Pandis, I. Riipinen, Y. Rudich, M. Schaap, J.G. Slowik, D.V. Spracklen, E. Vignati, M. Wild, M. Williams, S. Gilardoni, Particulate matter, air quality and climate: lessons learned and future needs, Atmos. Chem. Phys. 15 (14) (2015) 8217–8299.
[3] U. Pöschl, Atmospheric aerosols: composition, transformation, climate and health effects, Angew. Chem. Int. Ed. 44 (46) (2005) 7520–7540.
[4] I.E. Nielsen, H. Skov, A. Massling, A.C. Eriksson, M. Dall'Osto, H. Junninen, N. Sarnela, R. Lange, S. Collier, Q. Zhang, C.D. Cappa, J.K. Nøjgaard, Biogenic and anthropogenic sources of aerosols at the High Arctic site Villum Research Station, Atmos. Chem. Phys. 19 (2019) 10239–10256.
[5] J. Csavina, J. Field, M.P. Taylor, S. Gao, A. Landázuri, E.A. Betterton, A.E. Sáez, A review on the importance of metals and metalloids in atmospheric dust and aerosol from mining operations, Sci. Total Environ. 433 (2012) 58–73.
[6] A. Nel, Air pollution-related illness: effects of particles, Science 308 (2005) 804.
[7] IPCC, Climate Change 2013: The Physical Science Basis. Contribution of Working Group I to the Fifth Assessment Report of the Intergovernmental Panel on Climate Change, Cambridge University Press, Cambridge, United Kingdom and New York, NY, USA, 2013.
[8] C. Marina-Montes, L.V. Pérez-Arribas, M. Escudero, J. Anzano, J.O. Cáceres, Heavy metal transport and evolution of atmospheric aerosols in the Antarctic region, Sci. Total Environ. 721 (2020) 137702.
[9] M. Hallquist, J.C. Wenger, U. Baltensperger, Y. Rudich, D. Simpson, M. Claeys, J. Dommen, N.M. Donahue, C. George, A.H. Goldstein, J.F. Hamilton, H. Herrmann, T. Hoffmann, Y. Iinuma, M. Jang, M.E. Jenkin, J.L. Jimenez, A. Kiendler-Scharr, W. Maenhaut, G. McFiggans, T.F. Mentel, A. Monod, A.S.H. Prévôt, J.H. Seinfeld, J.D. Surratt, R. Szmigielski, J. Wildt, The formation, properties and impact of secondary organic aerosol: current and emerging issues, Atmos. Chem. Phys. 9 (14) (2009) 5155–5236.
[10] D. Cajiao, B. Albertos, P. Tejedo, L. Muñoz-Puelles, R. Garilleti, F. Lara, L.G. Sancho, D.G. Tirira, D. Simón-Baile, G.K. Reck, C. Olave, J. Benayas, Assessing the conservation values and tourism threats in Barrientos Island, Antarctic Peninsula, J. Environ. Manage. 266 (2020) 110593.
[11] E.Y. Osipov, O.P. Osipova, T.V. Khodzher, Recent variability of atmospheric circulation patterns inferred from East Antarctica glaciochemical records, Geochemistry 80 (3) (2020) 125554, https://doi.org/10.1016/j.chemer.2019.125554.
[12] M. Legrand, S. Preunkert, R. Weller, L. Zipf, C. Elsässer, S. Merchel, G. Rugel, D. Wagenbach, Year-round record of bulk and size-segregated aerosol composition in central Antarctica (Concordia site) – Part 2: Biogenic sulfur (sulfate and methanesulfonate) aerosol, Atmos. Chem. Phys. 17 (2017) 14055–14073.
[13] G. Xu, L. Chen, M. Zhang, Y. Zhang, J. Wang, Q. Lin, Year-round records of bulk aerosol composition over the Zhongshan Station, Coastal East Antarctica, Air Qual. Atmos. Health 12 (2019) 271–288.
[14] S. Decesari, M. Paglione, M. Rinaldi, M. Dall'Osto, R. Simó, N. Zanca, F. Volpi, M. C. Facchini, T. Hoffmann, S. Götz, C.J. Kampf, C. O'Dowd, D. Ceburnis, J. Ovadnevaite, E. Tagliavini, Shipborne measurements of Antarctic submicron organic aerosols: an NMR perspective linking multiple sources and bioregions, Atmos. Chem. Phys. 20 (2020) 4193–4207.
[15] J.O. Cáceres, D. Sanz-Mangas, S. Manzoor, L.V. Pérez-Arribas, J. Anzano, Quantification of particulate matter, tracking the origin and relationship between elements for the environmental monitoring of the Antarctic region, Sci. Total Environ. 665 (2019) 125–132.
[16] C. Marina-Montes, L.V. Pérez-Arribas, J. Anzano, J.O. Cáceres, Local and Remote Sources of Airborne Suspended Particulate Matter in the Antarctic Region, Atmosphere 11 (4) (2020) 373, https://doi.org/10.3390/atmos11040373.
[17] S. Sobanska, G. Falgayrac, J. Rimetz-Planchon, E. Perdrix, C. Brémard, J. Barbillat, Resolving the internal structure of individual atmospheric aerosol particle by the combination of Atomic Force Microscopy, ESEM–EDX, Raman and ToF–SIMS imaging, Microchem. J. 114 (2014) 89–98.
[18] Q.i. Zhang, J.L. Jimenez, M.R. Canagaratna, I.M. Ulbrich, N.L. Ng, D.R. Worsnop, Y. Sun, Understanding atmospheric organic aerosols via factor analysis of aerosol mass spectrometry: a review, Anal. Bioanal. Chem. 401 (10) (2011) 3045–3067.
[19] H. Cheng, X. Dong, Y. Yang, Y. Feng, T. Wang, M.A. Tahir, L. Zhang, H. Fu, Au nanoring arrays as surface enhanced Raman spectroscopy substrate for chemical component study of individual atmospheric aerosol particle, J. Environ. Sci. 100 (2021) 11–17.
[20] C. Marina-Montes, V. Motto-Ros, L.V. Pérez-Arribas, J. Anzano, M. Millán-Martínez, J.O. Cáceres, Aerosol analysis by micro laser-induced breakdown spectroscopy: A new protocol for particulate matter characterization in filters, Anal. Chim. Acta 1181 (2021) 338947.
[21] R.L. Craig, L. Nandy, J.L. Axson, C.S. Dutcher, A.P. Ault, Spectroscopic determination of aerosol pH from acid-base equilibria in inorganic, organic, and mixed systems, J. Phys. Chem. A 121 (2017) 5690–5699.
[22] H.J. Eom, D. Gupta, H.R. Cho, H.J. Hwang, S.D. Hur, Y. Gim, C.U. Ro, Single-particle investigation of summertime and wintertime Antarctic sea spray

aerosols using low-Z particle EPMA, Raman microspectrometry, and ATR-FTIR imaging techniques, Atmos. Chem. Phys. 16 (2016) 13823–13836.
[23] D. Gupta, H.J. Eom, H.R. Cho, C.U. Ro, Hygroscopic behavior of NaCl–MgCl₂ mixture particles as nascent sea-spray aerosol surrogates and observation of efflorescence during humidification, Atmos. Chem. Phys. 15 (2015) 11273–11290.
[24] S.K. Sze, N. Siddique, J.J. Sloan, R. Escribano, Raman spectroscopic characterization of carbonaceous aerosols, Atmos. Environ. 35 (2001) 561–568.
[25] Y. Feng, L. Liu, Y. Yang, Y. Deng, K. Li, H. Cheng, X. Dong, W. Li, L. Zhang, The application of Raman spectroscopy combined with multivariable analysis on source apportionment of atmospheric black carbon aerosols, Sci. Total Environ. 685 (2019) 189–196.
[26] J.I. Goldstein, D.E. Newbury, P. Echlin, D.C. Joy, C.E. Lyman, E. Lifshin, J.R. Michael, Scanning Electron Microscopy and X-ray Microanalysis, in: D.E. Newbury, Echlin, P., Joy, D. C., Lyman, C. E., Lifshin, E., ... Michael, J. R. (Ed.), Springer US, 2003.
[27] J. Toporski, T. Dieing, O. Hollricher, Confocal Raman Microscopy. Springer Series in Surface Sciences, in, Springer International Publishing, 2018.
[28] C. Cardell, I. Guerra, An overview of emerging hyphenated SEM-EDX and Raman spectroscopy systems: Applications in life, environmental and materials sciences, TrAC, Trends Anal. Chem. 77 (2016) 156–166.
[29] DIN-EN-12341, Ambient air - Standard gravimetric measurement method for the determination of the PM<(Index)>10N or PM<(Index)>2,5N mass concentration of suspended particulate matter., in, In:Standard, E. (Ed.), DIN EN 12341, 2014, pp. 57.
[30] K. Castro, M. Pérez-Alonso, M.D. Rodríguez-Laso, L.A. Fernández, J.M. Madariaga, On-line FT-Raman and dispersive Raman spectra database of artists' materials (e-VISART database), Anal. Bioanal. Chem. 382 (2005) 248–258.
[31] B. Lafuente, R.T. Downs, H. Yang, N. Stone, The power of databases: The RRUFF project, in: Highlights in Mineralogical Crystallography, 2016, pp. 1-29.
[32] M. González-Pleiter, D. Velázquez, C. Edo, O. Carretero, J. Gago, Á. Barón-Sola, L. E. Hernández, I. Yousef, A. Quesada, F. Leganés, R. Rosal, F. Fernández-Piñas, Fibers spreading worldwide: Microplastics and other anthropogenic litter in an Arctic freshwater lake, Sci. Total Environ. 722 (2020) 137904.
[33] S. Allen, D. Allen, V.R. Phoenix, G. Le Roux, P. Durántez Jiménez, A. Simonneau, S. Binet, D. Galop, Atmospheric transport and deposition of microplastics in a remote mountain catchment, Nat. Geosci. 12 (2019) 339–344.
[34] M. González-Pleiter, C. Edo, D. Velázquez, M.C. Casero-Chamorro, F. Leganés, A. Quesada, F. Fernández-Piñas, R. Rosal, First detection of microplastics in the freshwater of an Antarctic Specially Protected Area, Mar. Pollut. Bull. 161 (2020) 111811.
[35] A. Cincinelli, C. Scopetani, D. Chelazzi, E. Lombardini, T. Martellini, A. Katsoyiannis, M.C. Fossi, S. Corsolini, Microplastic in the surface waters of the Ross Sea (Antarctica): Occurrence, distribution and characterization by FTIR, Chemosphere 175 (2017) 391–400.
[36] A.A. Sfriso, Y. Tomio, B. Rosso, A. Gambaro, A. Sfriso, F. Corami, E. Rastelli, C. Corinaldesi, M. Mistri, C. Munari, Microplastic accumulation in benthic invertebrates in Terra Nova Bay (Ross Sea, Antarctica), Environ. Int. 137 (2020) 105587.
[37] L. Bokobza, J.-L. Bruneel, M. Couzi, Raman Spectra of Carbon-Based Materials (from Graphite to Carbon Black) and of Some Silicone Composites, C, 1 (2015).
[38] A. Soewono, S. Rogak, Morphology and Raman Spectra of Engine-Emitted Particulates, Aerosol Sci. Technol. 45 (2011) 1206–1216.
[39] A. Ferrugiari, M. Tommasini, G. Zerbi, Raman spectroscopy of carbonaceous particles of environmental interest, J. Raman Spectrosc. 46 (2015) 1215–1224.
[40] E.B. Pereira, H. Evangelista, K.C.D. Pereira, I.F.A. Cavalcanti, A.W. Setzer, Apportionment of black carbon in the South Shetland Islands, Antarctic Peninsula, J. Geophys. Res.: Atmos. 111 (D3) (2006), https://doi.org/10.1029/2005JD006086.
[41] A.L. Khan, A.G. Klein, J.M. Katich, P. Xian, Local emissions and regional wildfires influence refractory black carbon observations near Palmer Station, Antarctica, Front. Earth Sci. 7 (2019) 49.
[42] E. Pino-Cortés, L.A. Díaz-Robles, F. Cubillos, F. Cereceda-Balic, R. Santander, J.S. Fu, S. Carrasco, J. Acosta, The black carbon dispersion in the Southern Hemisphere and its transport and fate to Antarctica, an Anthropocene evidence for climate change policies, Sci. Total Environ. 778 (2021) 146242.
[43] W.B. Lyons, C.A. Nezat, K.A. Welch, S.T. Kottmeier, P.T. Doran, Fossil Fuel Burning in Taylor Valley, Southern Victoria Land, Antarctica: Estimating the Role of Scientific Activities on Carbon and Nitrogen Reservoirs and Fluxes, Environ. Sci. Technol. 34 (2000) 1659–1662.
[44] K.A. Casey, S.D. Kaspari, S.M. Skiles, K. Kreutz, M.J. Handley, The spectral and chemical measurement of pollutants on snow near South Pole, Antarctica, J. Geophys. Res.: Atmos. 122 (2017) 6592–6610.
[45] S.G. Warren, A.D. Clarke, Soot in the atmosphere and snow surface of Antarctica, J. Geophys. Res.: Atmos. 95 (D2) (1990) 1811, https://doi.org/10.1029/JD095iD02p01811.
[46] IAATO, Report on IAATO Operator Use of Antarctic Peninsula Landing Sites and ATCM Visitor Site Guidelines, 2016-17 Season. IP 164., in, 2017.
[47] C. García-Florentino, L. Gomez-Nubla, J. Huidobro, I. Torre-Fdez, P. Ruíz-Galende, J. Aramendia, E.M. Hausrath, K. Castro, G. Arana, J.M. Madariaga, Interrelationships in the Gypsum–Syngenite–Görgeyite System and Their Possible Formation on Mars, Astrobiology 21 (3) (2021) 332–344.
[48] N. Prieto-Taboada, O. Gómez-Laserna, I. Martínez-Arkarazo, M.Á. Olazabal, J.M. Madariaga, Raman Spectra of the Different Phases in the CaSO4–H2O System, Anal. Chem. 86 (2014) 10131–10137.
[49] N. Prieto-Taboada, S. Fdez-Ortiz de Vallejuelo, M. Veneranda, I. Marcaida, H. Morillas, M. Maguregui, K. Castro, E. De Carolis, M. Osanna, J.M. Madariaga, Study of the soluble salts formation in a recently restored house of Pompeii by in-situ Raman spectroscopy, Sci. Rep. 8 (2018) 1613.
[50] R.L. Frost, A Raman spectroscopic study of copiapites Fe2+Fe3+(SO4)6(OH)2 · 20H2O: environmental implications, J. Raman Spectrosc. 42 (5) (2011) 1130–1134.
[51] G. Wollmann, D. Freyer, W. Voigt, Polyhalite and its analogous triple salts, Monatshefte für Chemie - Chemical Monthly 139 (2008) 739–745.
[52] S.F. Parker, L. Zhong, Vibrational spectroscopy of metal methanesulfonates: M = Na, Cs, Cu, Ag, Cd, Royal Soc. Open Sci. 5 (4) (2018) 171574, https://doi.org/10.1098/rsos.171574.
[53] F. Zapata, F. Ortega-Ojeda, C. García-Ruiz, M. González-Herráez, Selective Monitoring of Oxyanion Mixtures by a Flow System with Raman Detection, Sensors 18 (2018) 2196.
[54] J. Eichler, C. Weikusat, A. Wegner, B. Twarloh, M. Behrens, H. Fischer, M. Hörhold, D. Jansen, S. Kipfstuhl, U. Ruth, F. Wilhelms, I. Weikusat, Impurity Analysis and Microstructure Along the Climatic Transition From MIS 6 Into 5e in the EDML Ice Core Using Cryo-Raman Microscopy, Front. Earth Sci. 7 (2019), https://doi.org/10.3389/feart.2019.0002010.3389/feart.2019.00020.s001.
[55] M. Zhang, L. Chen, G. Xu, Q. Lin, M. Liang, Linking Phytoplankton Activity in Polynyas and Sulfur Aerosols over Zhongshan Station, East Antarctica, J. Atmos. Sci. 72 (2015) 4629–4642.
[56] H. Bao, D.A. Campbell, J.G. Bockheim, M.H. Thiemens, Origins of sulphate in Antarctic dry-valley soils as deduced from anomalous 17O compositions, Nature 407 (6803) (2000) 499–502.
[57] S. Kumar, R. Gopinathan, G.K. Chandra, S. Umapathy, D.K. Saini, Rapid detection of bacterial infection and viability assessment with high specificity and sensitivity using Raman microspectroscopy, Anal Bioanal Chem 412 (11) (2020) 2505–2516.
[58] C.-S. Ho, N. Jean, C.A. Hogan, L. Blackmon, S.S. Jeffrey, M. Holodniy, N. Banaei, A. A.E. Saleh, S. Ermon, J. Dionne, Rapid identification of pathogenic bacteria using Raman spectroscopy and deep learning, Nat. Commun. 10 (2019) 4927.
[59] S.D.J. Archer, K.C. Lee, T. Caruso, T. Maki, C.K. Lee, S.C. Cary, D.A. Cowan, F.T. Maestre, S.B. Pointing, Airborne microbial transport limitation to isolated Antarctic soil habitats, Nature, Microbiology 4 (6) (2019) 925–932.
[60] E. Mayol, J.M. Arrieta, M.A. Jiménez, A. Martínez-Asensio, N. Garcias-Bonet, J. Dachs, B. González-Gaya, S.-J. Royer, V.M. Benítez-Barrios, E. Fraile-Nuez, C.M. Duarte, Long-range transport of airborne microbes over the global tropical and subtropical ocean, Nat. Commun. 8 (2017) 201.
[61] E. Mayol, M.A. Jiménez, G.J. Herndl, C.M. Duarte, J.M. Arrieta, Resolving the abundance and air-sea fluxes of airborne microorganisms in the North Atlantic Ocean, Front. Microbiol. 5 (2014) 557.